The role of intersystem crossing in the reactive collision of $S^+(^4S)$ with H_2

Alexandre Zanchet, Octavio Roncero, Ezman Karabulut, Nicolas Solem, Claire Romanzin, Roland Thissen, Christian Alcaraz

▶ **To cite this version:**

Alexandre Zanchet, Octavio Roncero, Ezman Karabulut, Nicolas Solem, Claire Romanzin, et al.. The role of intersystem crossing in the reactive collision of $S^+(^4S)$ with H_2. The Journal of Chemical Physics, 2024, 161 (4), pp.044302. 10.1063/5.0214447 . hal-04658975

HAL Id: hal-04658975
https://hal.science/hal-04658975v1

Submitted on 22 Jul 2024

HAL is a multi-disciplinary open access archive for the deposit and dissemination of scientific research documents, whether they are published or not. The documents may come from teaching and research institutions in France or abroad, or from public or private research centers.

L'archive ouverte pluridisciplinaire **HAL**, est destinée au dépôt et à la diffusion de documents scientifiques de niveau recherche, publiés ou non, émanant des établissements d'enseignement et de recherche français ou étrangers, des laboratoires publics ou privés.

Copyright

The role of intersystem crossing in the reactive collision of $S^+(^4S)$ with H_2.

Alexandre Zanchet[a] and Octavio Roncero
Instituto de Física Fundamental, CSIC, Serrano 123, 28006, Madrid, Spain
Ezman Karabulut
Vocational School of Health Services, Bitlis Eren University, 13000 Bitlis, Turkey
Nicolas Solem, Claire Romanzin, Roland Thissen, and Christian Alcaraz
Université Paris-Saclay, CNRS, Institut de Chimie Physique,UMR8000,91405 Orsay, France and
Synchrotron SOLEIL, L'Orme des Merisiers,91192 Saint Aubin,Gif-sur-Yvette, France

(Dated: 21 June 2024)

We report a study on the reactive collision of $S^+(^4S)$ with H_2, HD and D_2 combining guided ion beam experiment and quantum-mechanical calculations. It is found that the reactive cross sections reflect the existence of two different mechanisms, one being spin-forbidden. Using different models we demonstrate that the spin-forbidden pathway follows a complex mechanism involving three electronic states instead of two as previously thought. The good agreement between theory and experiment validates the methodology employed and allows to fully understand the reaction mechanism. This study also provides new fundamental insights on the intersystem crossing process.

I. INTRODUCTION

Intersystem crossing (ISC) is a radiationless process involving a transition between two electronic states of different spin multiplicity. The coupling between different electronic states can then lead to non-adiabatic processes which are known to play a significant role in numerous fields, like photochemistry where they often play a crucial role in the reaction dynamics occuring in the excited electronic states[1,2], biological processes like photosynthesis[3] and in several medical and technological applications such as photodynamic cancer therapy[4], organic light-emitting diodes (OLED)[5] or the catalytic activation of molecular oxygen[6], among others.

This radiationless process was first studied empiricaly by El-Sayed in the early sixties[7] when spectroscopy technics started to be employed to study the response of complex molecules to light[8]. But it is in photochemistry at the end of eighties and the advent of femtosecond spectroscopy[9] that a step forward in the understanding of this process could be achieved. Indeed, for a long time it was thought that ISC was a slow process in organic compounds compared to the spin-allowed internal conversion (IC), and its contribution was often neglected in the dynamics of excited electronic states. Several femtosecond resolved experiments could however demonstrate that ISC can occur in a sub-picosecond time scale and can thus be competitive with IC, even in molecules composed only of light atoms[8]. In the nineties, simulations combining quantum chemistry and nuclei dynamics[10,11] also contributed to a better understanding of this process and lay the first stone to non-adiabatic molecular dynamics including Spin-Orbit Couplings (SOCs). Nowadays, spin-orbit effects are included in several reaction dynamics approaches suitable at different size scales. Most studies are performed relying on classical trajectories which include Surface Hopping between electronic states, also known as Trajectory Surface Hopping (TSH). This approach is implemented in QM/MM[12], *on-the-fly ab initio dynamics*[13] and Quasi-Classical Trajectories (QCT)[14]. The SOCs can also be accounted more accurately using quantum approaches where the population transfer between electronic states is formally taken in account such as Multi Configuration Time Dependent Hartree (MCTDH)[15] and exact Wave Packet Time Dependent Reaction Dynamics (WP)[16], the latter being limited to very small systems. The insight given by these theoretical studies combined to the experimental findings allowed to demonstrate that the ISC does not only depend on the direct spin-orbit interaction as previously thought, but that nuclei motion also plays an important role so that ISC can be seen as a spin-vibronic mechanism[8]. Those findings also permited to derive the Non-Adiabatic Transition State Theory (NA-TST)[17], a statistical approach widely used for calculating the rate of intersystem crossings in large systems such as active sites of proteins[18].

Most of the studies related to ISC are associated to photochemistry and therefore to dynamics on the excited electronic states. Studies on the effect of ISC on reactive scattering between species in the ground state are however scarce. Schatz and coworkers studied the effect of ISC in the reactions $O+H_2$[19] and $S+H_2$[20] applying surface hopping QCT and accounting for the SOCs with a sophisticated model. The ISC in the $O+H_2$ reaction was also studied by exact quantum wave packet study by K.-L. Han and coworkers[21], but these theoretical predictions could not be compared to experiment. More experimental studies can be found for larger systems, in particular by Casavecchia and coworkers who studied ISC in several reactions between atomic $O(^3P)$ with several

[a] Electronic mail: alexandre.zanchet@csic.es

unsaturated hydrocarbons[22]. The ISC in one of these reactions, $O(^3P)+C_2H_4$, motivated numerous theoretical studies on the electronic stucture[23] and reaction dynamics studies using TSH[24,25] and NA-TST[26]. Although theory could qualitatively explain the experimental observation, it was not able to reproduce quantitatively the experimental branching ratio between products. With a system of 15 degrees of freedom (seven atoms), too many approximations are necessary to treat the reaction dynamics so it is difficult to determine if the discrepancy arises from the quality of the Potential Energy Surface (PES) and the accuracy of the couplings, or if it is an intrisic problem of the approximations assumed in the TSH or NA-TST methods. Indeed, spin orbit interactions are governed by strict selection rules and properly taking them into account remains a challenge for theoreticians as several electronic states have to be considered simultaneously, and since the spin-orbit couplings (SOCs) are vectorial quantities[27], they are also sensitive to the rotation of the system. Due to this complexity, it is impossible to consider an exact model accounting perfectly for all aspects of the spin-orbit interactions in polyatomic systems. However, it is still possible to build a rigorous model in the case of triatomic systems.

Interestingly, reaction between sulfur cation and molecular hydrogen, a triatomic system, is a good candidate to study ISC in detail. In the experimental study of Stowe *et al.*[28] on $S^+ + H_2 \rightarrow SH^+ + H$ and its isotopologues, the cross section associated to $S^+(^4S)$ show two maxima that can be clearly differentiated after substraction of the contribution of the $S^+(^2D)$ on the total cross section. The two maxima were interpreted as a signature of two competing mechanisms, one spin-allowed mechanism occurring on the quartet state and one spin-forbidden involving an ICS to the $^2\tilde{X}$ state of H_2S^+. Evidences of spin-forbidden predissociation through the $^4A''$ state to produce S^+ were also reported in photochemical experiments probing the $^2\tilde{X}$ and $^2\tilde{A}$ states of H_2S^+,[29–32] suggesting that the $^2\tilde{A}$ state may also play a role in the reaction mechanism. More recently, a combined theory/experiment study on the photodissociation of H_2S^+ also confirmed the existence of several mechanisms in the photofragmentation dynamics, some of them involving the three electronic states and mediated by spin-orbit couplings in the photodissociation dynamics.[33] For the reactive collision $S^+ + H_2$ however, while the reaction dynamics of the spin allowed mechanism have been studied extensively theoretically in the last decade[34–41] and is now well understood, no theoretical work have been able to reproduce the signal associated with the spin-forbidden pathway which remains uncertain.

To confirm and understand how ISCs affect the reaction, we present a new study combining theory and experiment on the collision between S^+ cation in its ground spin-orbit state with different molecular hydrogen isotopologues. The experiment performed originally by Stowe *et al.*[28] will be revisited for both HD and D_2 with a source of pure $S^+(^4S)$ with no $S^+(^2D)$ contamination, and will be complemented with the results of the collision with H_2 for which no experimental data are available. The experimental measurements will be compared to the results obtained by three sets of WP calculations. Finally, the comparison of the different models with experimental data will allow to fully derive the reaction mechanism of both spin-allowed and spin-forbidden pathways producing SH^+. Solid conclusions will then be drawn allowing a better general comprehension on the ISC process.

II. EXPERIMENT

The three ion-molecule reactions $S^+(^4S) + H_2$, $S^+(^4S) + HD$ and $S^+(^4S) + D_2$ have been studied experimentally on the CERISES setup[42,43] attached on the DESIRS beamline[44] at the French synchrotron SOLEIL. CERISES is a Guided Ion Beam (GIB) setup based on a sequence of 4 radio frequency (RF) devices: quadrupole-octopole-octopole-quadrupole (QOOQ) allowing the mass selection (Quad 1) of parent cations produced in a source by photoionization or dissociative photoionization of precursors with VUV synchrotron radiation, the control of the collision energy and the reaction (Oct 1) with the target gas and finally the mass selection (Quad 2) of the unreacted parent ions (S^+) and product ions (SH^+ or SD^+) before their detection. Absolute reaction cross sections are extracted from the measured ion yields and the absolute pressure of the target gas that are set to insure the single collision regime, using the calibration reaction $Ar^+ + D_2 \rightarrow ArD^+ + D$ to get the effective cell length.[45]

The dissociative photoionization of CS_2 has been found to be the more direct and easy way to produce the sulfur atomic ions, S^+. For this, CERISES was attached to the DESIRS beamline[44] at the French synchrotron SOLEIL producing monochromatized VUV (vacuum ultra-violet) photons typically between 6 and 40 eV. On Figure 1 are displayed the ion yields of the CS_2^+ precursor ion (m/z 76) and the $^{32}S^+$ atomic ion (m/z 32) together with the threshold photoelectron (TPE) spectrum. TPE are very slow photoelectrons (kinetic energies below 20 meV here) extracted from the source with small fields (≈ 1 V) which allow the discrimination of fast electrons, both geometrically and temporally[42,43]. They are very useful to characterize the photoionization of CS_2, as seen on the lower panel of Figure 1 where electronic states of CS_2^+ have been identified, contrary to the CS_2^+ yield (top panel) which exhibits complex autoionization structures due to highly excited (Rydberg) states of the neutral CS_2. On the middle panel showing the $^{32}S^+$ ion yield, it is visible that above a threshold of about 14.8 eV, S^+ can be produced at rates higher than several 1000s ions/sec. We have added the three expected limits for the production of $S^+(^4S) + CS$, $S^+(^2D) + CS$ and $S^+(^2P) + CS$. Clearly, S^+ ions appear at the first expected limit associated with the ground state $S^+(^4S)$. Setting the photon energy on

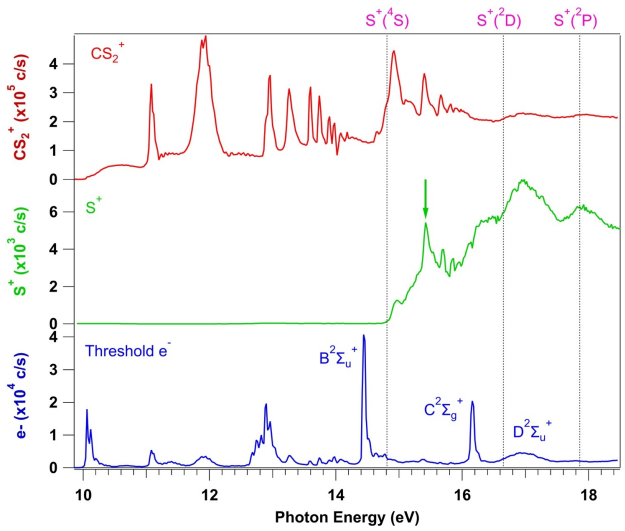

FIG. 1. Photoionization and dissociative photoionization of CS_2. Top and middle panels: mass selected CS_2^+ and S^+ ion yields at m/z 76 (red) and 32 (green) respectively. Bottom panel: threshold photoelectron spectrum (blue). The three limits for the production of $S^+(^4S)$ + CS, $S^+(^2D)$ + CS, $S^+(^2P)$ + CS are indicated by vertical black dashed lines.

the well defined peak at about 15.4 eV allows the production of S^+ ions at large rates while ensuring the formation of pure ground state $S^+(^4S)$ without any contamination by electronically excited $S^+(^2D)$ or $S^+(^2P)$ ions. This is the photon energy at which we have chosen to study the three reactions.

The conducted measurements posed a challenge concerning the kinetic energy (lab) necessary to observe the endothermic process and elucidate its cross section at higher energy levels. To achieve energies up to 13 eV in the center-of-mass frame when colliding $^{32}S^+$ with H_2, ion acceleration in the lab frame up to $13 \times (32+2)/2 = 221$ eV was essential. This acceleration was facilitated through the utilization of new digital power supplies, specifically three modules of ISEG EBS (12 channels, +/- 500 V Bipolar Quadrants). These modules supplied all the DC potentials required for instrument tuning and operation. The standard measurement approach in the CERISES setup involves optimizing all the lens elements for maximal transmission and adjusting the potential of the first octupole and subsequent elements to reach the desired collision energy. This adjustment is accomplished by floating one of the ISEG modules at the potential of a retarding potential, generated by a computer-controlled PCI 6704 board (+/- 10V with 16 bits precision), amplified up to 60 V by a x6 DC/DC amplifier. Given the higher potentials necessary for the current measurements, one channel from the non-floating ISEG modules was used to supply the floating module with the required potential (this induced the need to slow down the acquisition of retarding potential spectra as up to 1 s is needed to establish the exact potential). Additionally, it is recognized that the mass resolution of quadrupole mass filters diminishes significantly when mass-selected ions possess high kinetic energy. As the present measurements required a mass separation of 1 or 2 u ($^{32}S^+$ vs $^{32}SH^+$ or $^{32}SD^+$), it became imperative to reconsider the conventional floating potential method. This revision was crucial to enable the filtering of product ions and parent ions in the second quadrupole, even with kinetic energies as high as 221 eV. Consequently, the potential of the second quadrupole was prevented from floating and fixed between -16 and -24 V relative to the center of the ion source. By calculating the kinetic energies of the product ions in the lab frame (E'_{Lab1}) at the most critical point, i.e. in the 2nd quadrupole (QuadII), we have found that no product ions are discriminated for collision energies lower than 6.0 eV for S^++H_2, 9.2 eV for S^++D_2, and 8.1 and 10.4 eV for S^++HD producing respectively SH^++D and SD^++H, even in the worst case for which the SH^+/SD^+ products are scattered backward relative to the S^+ parent (scattering angle 180° in the CM frame). For higher ECMs, the maximum angle at which no product ions are discriminated can be lower than 180° and depending on the differential cross section as a function of theta, some product ions are gradually discriminated, and we should expect a decrease of transmission of these products with increasing ECM.

III. THEORY

Reaction dynamics of S^++H_2, S^++HD and S^++D_2 have been studied for collision energies up to 3 eV using Exact Time Dependent Wave Packet (WP) calculations on several sets of spin-orbit coupled Potential Energy Surfaces of MRCI/AV5Z quality.

A. Spin-orbit couplings

To treat properly spin-orbit interactions, the complex electronic structure of the H_2S^+ system has to be well understood, characterizing the orbital and spin angular momenta of the electronic states from reactants, complex and products, and establishing the correlations between these different regions. In Fig. 2, the correlation diagram of the H_2S^+ is presented. It appears that only the $^4A''$ state correlates the ground states of reactants and products, without possibility to form a complex. On the other hand, the $\tilde{X}^2A''$ and $\tilde{A}^2A'$ states of H_2S^+, both correlating to the excited state of sulfur cation $S^+(^2D)$, can form stable complexes lower in energies than the reactant channel $S^+(^4S)$+H_2. Like the quartet state, the $\tilde{X}^2A''$ state correlates to the ground state of products while the $\tilde{A}^2A'$ state correlates to an excited state of SH^+. Both doublet states have thus to cross the quartet state at some point, favorising the possibility of ISC.

Once the correlation of the electronic states is established, the next step is to study their spin-orbit contri-

butions and their couplings. In the asymtotic regions, atoms and diatomic molecules present orbital ($\mathbf{L}/\Lambda$) and spin (S) electronic momentum whose projections are well defined, so the spin-orbit contributions and couplings can be easily derived. This is not the case in the region of the complex since outside colinearity the electronic wavefunctions are mixed and consequently, orbital angular momentum is no longer defined. This is particulary relevant because when the dominant character of the electronic wavefunction changes, the value of $\mathbf{L}$ changes accordingly, and consequently the SOCs too. This changes can become important near avoided crossings and critical near conical intersections. As a result, in the adiabatic representation, SOCs may not be continue and derivable over the whole configuration space, and in such cases cannot be fitted accurately. It is thus necessary to construct an approximate model which account for the most relevant aspects to reproduce the physics of the system while getting rid of numerical artifacts that may arise from the disconitnuities in the SOCs.

To understand properly the evolution of the couplings, we looked at the behaviour of the different electronic states in colinear configuration where the orbital angular momentum $\mathbf{L}$ is well defined and followed their evolution with the bending angle. In figure 3, approximate reaction paths of six doublet states have been computed at CASSCF level for different bending angles. Calculations were performed using the H-H-S internal coordinates, to follow the evolution of the electronic states from reactants to products. In the entrance channel $S^+ + H_2$, the interaction is attractive for the Π state, but the Π states appears as a high lying excited state of SH^+. As a consequence, along the reaction path, the Π state crosses

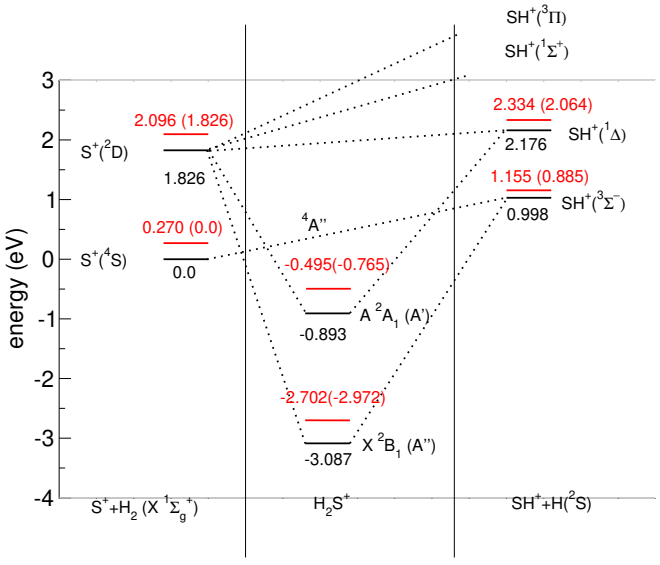

FIG. 2. Adiabatic correlation diagram of the SH_2^+ system. The Zero Point Energies in the case of non deuterated species are shown in red and the energies refered to H_2(v=0, j=0) are shown in parenthesis.

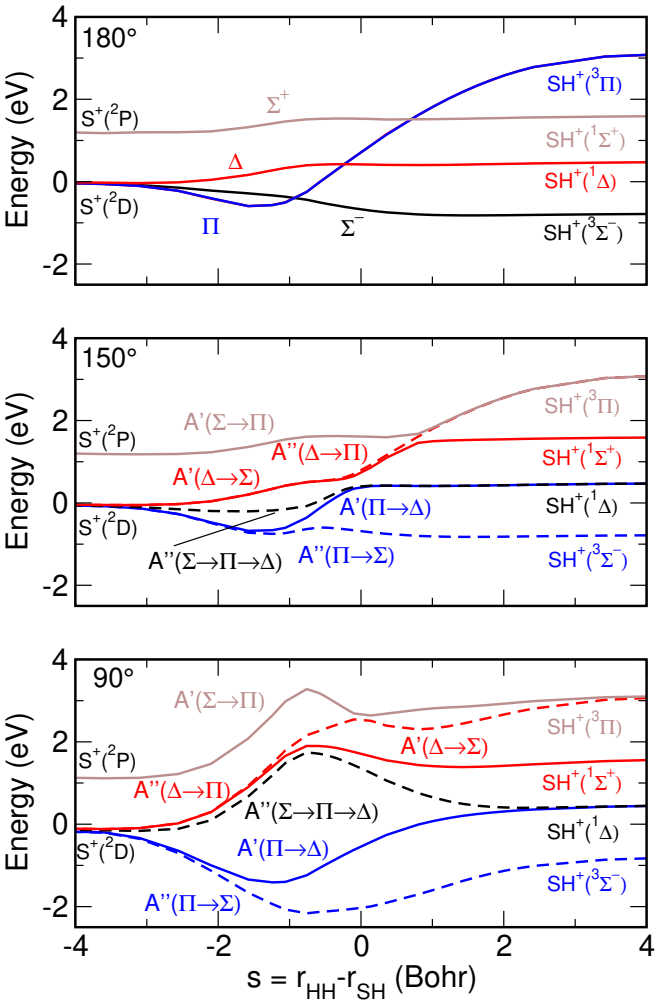

FIG. 3. Reaction path for several bending angles H-H-S. The reaction coordinate is defined as the difference between HH and SH distances. For the colinear case, the genuine $C_{\infty v}$ notation is employed. For bent cases, solid lines corresponds to states of A' symmetry in the C_s group while dashed lines corresponds to states of A'' symmetry. The evolution of the dominant character of the electronic wavefunction is also shown.

the Σ^- and Δ states, and even an additional Σ^+ state arising from the ^2P state of S^+. Outside colinearity, the degereneracies of the Π and Δ states are lifted, and it can be appreciated in figure 3 how the the different electronic states along the reaction paths are modified with the $\widehat{HHS}$ angle. In the region of the wells, which corresponds to a conformation where the S^+ is inserted between the two H and which appears for small bending angles in the chosen coordinates, and no clear character can be defined. This implies that the different electronic angular momenta will be mixed in the region of the well so we can expect that SOCs will always be present in this region. Interestingly, this is not the case in the asymptotic regions, where independently of the bending angle, the dominant characters in the asymptotic regions are very similar to what is observed in the collinear case.

Assuming a three state model, the SOCs were calculated using the MOLPRO package[46] on a regular grid of points in the reactant Jacobi coordinates **r**, **R** and γ, where **r** is the vector between the two H atoms, **R** is the vector between the center of mass of H_2 and S^+ and γ the angle between the two vectors. The grid was chosen to cover the crossing seams between the $^4A''$ and both $^2A'/^2A''$ states. The values of the points of the grid are r=[1.0, 1.2, 1.4, 1.6, 1.8, 2.0, 2.2, 2.4 2.6, 3.0] Bohr, R=[3.0, 3.2, 3.4, 3.6, 3.8, 4.0, 4.2, 4.4, 4.6, 4.8, 5.0] Bohr and γ= [0, 15, 30, 45, 60, 75, 90] degrees. For each point of the grid, a CASSCF[47] calculation was performed considering 5 doublet states (2 A'+3 A'') and the quartet state with the same active space used to constructed the adiabatic PESs[37]. The CASSCF calculation is then followed by a MRCI treatment[48] where only the first electronic state of $^4A''$, $^2A'$ and $^2A''$ representations are calculated. Then, the 8×8 spin-orbit matrix associated to these three states is calculated using the Breit-Pauli operator as implemented in MOLPRO[49]. The general form of the matrix is:

$$\begin{pmatrix}
{}^4A''_{3/2} & 0 & 0 & 0 & V'_{3/2,1/2} & 0 & V''_{3/2,1/2} & 0 \\
0 & {}^4A''_{1/2} & 0 & 0 & 0 & V'_{1/2,-1/2} & 0 & V''_{1/2,-1/2} \\
0 & 0 & {}^4A''_{-1/2} & 0 & V'_{1/2,-1/2} & 0 & -V''_{1/2,-1/2} & 0 \\
0 & 0 & 0 & {}^4A''_{-3/2} & 0 & V'_{3/2,1/2} & 0 & -V''_{3/2,1/2} \\
V'_{3/2,1/2} & 0 & V'_{1/2,-1/2} & 0 & {}^2A'_{1/2} & 0 & -V^{\Pi}_{1/2,1/2} & -V^{\Sigma}_{1/2,-1/2} \\
0 & V'_{1/2,-1/2} & 0 & V'_{3/2,1/2} & 0 & {}^2A'_{-1/2} & V^{\Sigma}_{1/2,-1/2} & V^{\Pi}_{1/2,1/2} \\
-V''_{3/2,1/2} & 0 & V''_{1/2,-1/2} & 0 & V^{\Pi}_{1/2,1/2} & V^{\Sigma}_{1/2,-1/2} & {}^2A''_{1/2} & 0 \\
0 & -V''_{1/2,-1/2} & 0 & V''_{3/2,1/2} & -V^{\Sigma}_{1/2,-1/2} & -V^{\Pi}_{1/2,1/2} & 0 & {}^2A''_{-1/2}
\end{pmatrix}$$

where the diagonal elements correspond to the MRCI adiabatic energies labeled by their respective symmetry and spin and the V terms refer to the different SOC elements. The SOCs labeled V' and V'' are those who couple the quartet ground state to both doublet states, those labeled V^{Π} and V^{Σ} couple the $^2A'$ and $^2A''$ states. The subindices refer to the projection Ω.

Since the orbital momentum of the $^4A''$ state is zero, V' and V'' can only be active when the doublet state present a Π character and will vanish in the regions of the PES where the charater is lost. The nature of V^{Π} and V^{Σ} is less intuitive since they refer to SOCs able to couple electronic state of same spin. This can be rationalized because in the adiabatic representation, the A' state is, by construction, linear combinations of $\Pi_{\Lambda=1}$ and $\Pi_{\Lambda=-1}$ (and/or $\Delta_{\Lambda=2}$ and $\Delta_{\Lambda=-2}$ depending of the region of the PES). So intrinsically, both $^2A'$ and $^2A''$ adiabatic states present the same spin and present, at least partially, contributions of the same orbital momentum projection Ω. Thus, part of the $^2A'$ and $^2A''$ states are always coupled (outside the particular case of the symmetric conformations $C_{\infty v}$ and C_{2v} where additional symmetry restrictions also apply). This statement is particularily interesting because, as discussed previously, in the region of the well, all the orbital angular momentum contributions are mixed in the electronic wavefunction. This would also be the case if more degrees of freedom were involved, so it should be a general case for polyatomic systems. This implies that non-zero SOCs, which may potentially lead to ISC, are always to be expected between doublet states. Surprisingly, we were not able to find any example in literature where the possibility of ISC between doublet states have been mentioned. The V^{Σ} terms also arise because of the mixing of character of the adiabatic wavefunction, but in this case, this term couples Σ and Π characters within the projection Ω=1/2. Unlike V^{Π}, this coupling term is thus not expected to affect the whole configuration space, as it will vanish when $^2A'$ loses its Π characters (exit channel) and when $^2A''$ does not present Σ character (entrance channel).

Since the Π character is lost along the reaction path, and the quartet/doublet crossing occurs in the entrance channel, V' and V'' are only relevant in this region, and the approximation of damping these couplings outside the entrance channel can be done, avoiding to fit the regions of these specific couplings terms where discontinuity may arise. The other coupling term expected to give problems of continuity is the V^{Σ}. However, due to its nature, it remains always small compared to V^{Π}. In our model, we thus decided to neglect this term in or-

der to simplify considerably the algebric as the problem can be separated into four uncoupled 3×3 matrices, one associated to each possible value of Ω. Accounting for symmetry properties (Ω = −3/2 and Ω = −1/2 are mirror images of Ω = 3/2 and Ω = 1/2), in practice we can consider only two of this matrices for the reaction dynamics calculations:

$$\begin{pmatrix} {}^4E'' & V''_{3/2} & V'_{3/2} \\ V''_{3/2} & {}^2E'' & V^{\Pi} \\ V'_{3/2} & V^{\Pi} & {}^2E' \end{pmatrix} \text{ and } \begin{pmatrix} {}^4E'' & V''_{1/2} & V'_{1/2} \\ V''_{1/2} & {}^2E'' & V^{\Pi} \\ V'_{1/2} & V^{\Pi} & {}^2E' \end{pmatrix}$$

These approximations greatly simplify the complexity and cost of the reaction dynamics calculation making it affordable while still allowing to grasp the major part of the effects of the SOCs on the production of SH^+. We should remark here that this approximation can be done only in the adiabatic representation. If a full diabatic representation were to be used, the full matrix would have to be considered.

B. Coupled Potential Energy Surfaces

To shed light on the effect of the SOCs, two coupled states models were considered in addition to a benchmark calculation on the uncoupled quartet states. In the first model, only the $^4A''$ and $^2A''$ states correlating with the ground state of SH^+ were considered. In the second model, the $^2A'$ electronic state is also considered. The models has been built as follow:

The spin-unperturbed adiabatic energies are given by the PESs of Zanchet *et al.*[37]. Then, the relevant couplings matrix elements for our model (V', V'' and V^{Π}) are calculated over a grid of points and fitted individually to build their respective analytical surface. The interpolation was performed using the Reproducing Kernel Hilbert Space (RKHS) method[50] using angle-like kernels, which are well adapted to grasp the angular dependance of the couplings[51]. The procedure is well described in other works[52,53], so here only the choice of the angle-like variables associated to the Jacobi coordinates will be described. The three angle-like variables were defined as $x = exp(-ar)$, $y = exp(-bR^2)$ and $z = (1 + cos(2\gamma))/2$. In the present case, the choice is $a = b = 0.1$.

The V^{Π} SOCs are relatively smooth and well behaved and were interpolated directly. However, an additional transformation had to be made to interpolate properly the V' and V'' SOCs. As mentioned previously, these SOCs vanish when the Π character of the doublet states is lost. The problem is that the transition is not smooth and does not occur at the same **r** value for different Jacobi angles, making them impossible to fit without obtaining artifacts. To solve this numerical problem, the SOCs have thus been divided by $\sin(\gamma)$ for **r** values larger than 1.9 Bohr before the interpolation (for smaller values of **r**, the Π character is always maintained and the coulings vanishes smoothly with **R**). Then the correct value is recovered simply by multiplying the interpolated value by $\sin(\gamma)$. This procedure allows to get rid of most of the artifacts generated by the interpolation, however, some residual errors remain at large **r** affecting the exit channel where these SOCs should have no relevant effects. This last problem was solved using a damping function when **r** is larger than 2.4 Bohr.

It appears that V' and V'' are rather similar for both M_J, which is expected since both states arise from the same Π state, which is their dominant character in the entrance channel. However, the SOCs related to Ω = 3/2 are larger than those related to Ω = 1/2 by nearly a factor of two. The maximum values for Ω= 3/2 and 1/2 are ≈ 180 cm^{-1} and ≈ 106 cm^{-1} respectively. Despite this difference in intensity, the shape of the SOCs is similar in both cases, and reach their maximum intensity for short **r** values and for **R**≈ 3 Bohr, which corresponds to the region of the crossing seam between the quartet and both doublet states. The V^{Π} coupling both doublet states are slightly stronger than the SOCs between quartet and doublet. They lie above 175 cm^{-1} in all the surface, with a maximum of ≈ 200 cm^{-1}, so unlike V' and V'', they are expected to be effective in the region of the H_2S^+ complex where the well of the $^2A'$ state is embedded inside the well of the $^2A''$. This SOC vanishes only when the three atoms are separated.

The maximum intensity of the SOCs are of the order of few hundreds of cm^{-1} while the global energetics of the title reactions is of the order of several eV. We can thus assume that spin orbit couplings will not affect significantly the energies of the spin-unperturbed adiabatic potentials. We can therefore apply an additional small approximation to our model by considering the pure spin-free adiabatics as the diagonal elements of our SO matrix, and the newly calculated SOCs as non-diagonal elements. Once all the different matrix elements are fitted, it is possible to construct the set of coupled PESs to be used in the dynamics.

C. Quantum reaction dynamics calculation

All the reaction dynamics calculations were realized using a quantum wave packet (WP) method implemented in the program MAD-WAVE3[54–60]. The WP propagation was performed using reactants Jacobi coordinates and use an efficient algorithm to transform the WP to product Jacobi coordinates at each iteration, as described in ref.[58]. The WP method allows to calculate the S-matrix elements for each value of J and ϵ, the total angular momentum and the parity, for a given set of initial state quantum numbers Γ_Ω, v, j, and ω where Γ_Ω is spin-orbit electronic state of symmetry Γ with total electronic angular momentum projection Ω, v is the vibrational quantum number, j is the rotational quantum number and ω, the projection of the nuclear total angular momentum. For a given energy E and for a given

electronic state Γ of projection Ω, the reaction probability is extracted from the S-matrix elements for each total nuclear angular momentum, J, and initial state, v, j as:

$$P^J_{\Gamma_\Omega vj}(E) = \frac{2}{2j+1} \sum_{\Gamma'_\Omega} \sum_{\omega\omega'} \sum_{v'j'\epsilon} \left| S^{J\epsilon}_{\Gamma_\Omega vj\omega,\Gamma_{\Omega'}v'j'\omega'}(E) \right|^2 \quad (1)$$

where Γ_Ω and Γ'_Ω refer to the initial and final spin-orbit states, vj and $v'j'$ to the initial and final rovibrational states, ω and ω' are the projections of the total nuclear angular momentum vector $\mathbf{J}$ and $\epsilon = \pm$. The helicity dependent cross-sections is defined as:[61,62]

$$\sigma_{\Gamma_\Omega vj\omega,\Gamma'_\Omega v'j'\omega'} = \frac{\pi}{k^2_{vj}} \sum_{J\epsilon} (2J+1) \left| S^{J\epsilon}_{\Gamma_\Omega vj\omega,\Gamma'_\Omega v'j'\omega'} \right|^2 \quad (2)$$

with $k^2_{vj} = 2\mu E/\hbar^2$ and $\mu = m_S m_{H_2}/(m_S + m_{H_2})$. The state to state cross section of the reaction $H_2(v,j)$ + S^+ $\rightarrow$ $HS^+(v',j')$+ H for a given energy can be obtained as the sum over the initial and final helicities ω and ω':

$$\sigma_{\Gamma_\Omega vj,\Gamma'_\Omega v'j'}(E) = \frac{1}{2j+1} \sum_{\omega,\omega'} \sigma_{\Gamma_\Omega vj\omega,\Gamma'_\Omega v'j'\omega'}(E) \quad (3)$$

The summation over all possible product states then gives the state specific cross section:

$$\sigma_{\Gamma_\Omega vj}(E) = \sum_{\Gamma'_\Omega} \sum_{v'j'} \sigma_{\Gamma_\Omega vj\omega,\Gamma'_\Omega v'j'\omega'} \quad (4)$$

In this work, we are interested in reactivity of $S^+(^4S)$, which correlates to four spin-orbit states (two doubly degenerate states: $\Omega = \pm 3/2$ and $\Omega = \pm 1/2$), so the total cross section for the reactants in their electronic ground state and rovibrational states vj is given by:

$$\sigma_{vj}(E) = \frac{1}{2} \sum_{\Gamma_\Omega > 0} \sigma_{\Omega vj}(E) \quad (5)$$

These calculations are particularly challenging because the deep wells of the doublet states, X^2A'' and A^2A', impose the use of dense grids and very long propagations. To converge the cross section up to 3 eV collision energy, a summation over all partial waves up to $J = 100$ for H_2 and D_2 and up to $J = 120$ for HD are necessary. Since the calculation for a given partial wave requires a large computational ressources, in order to save time and memory, calculations were only performed for partial waves multiple of 20. For intermediate values of J, $\left| S^{J\epsilon}_{\Gamma_\Omega vj\omega,\Gamma'_\Omega v'j'\omega'} \right|^2$ matrix elements were calculated using the J-shifting interpolation method[62,63]. For total angular momenta different from zero, the maximum helicity considered in the calculations is $\omega = 15$, which have been found sufficient to reach convergence. The parameters used in the WP calculations are listed in table I. These calculations are compared to WP calculations performed on the uncoupled $^4A''$ state to extract information on the ISC.

IV. RESULTS AND DISCUSSION

The dissociative photoionization of CS_2 at a photon energy of 15.4 eV has allowed the production of $S^+(^4S)$ with a 100% electronic purity (see section II for more details on the experiment). After extraction from the source, mass selection and control of their translational energy, $^{32}S^+$ cations have been collided with the target gas H_2 (and its isotopologues HD and D_2) at an absolute pressure of about 1.5 10^{-4} mbar, to study the bimolecular reaction $S^+(^4S)$ + H_2 (HD, D_2) under single collision conditions as a function of collision energy from thermal up to 15 eV in the Center of Mass (CM) frame. After a second mass selection, the intensity of the remaining parent ions and ionic products have been measured, from which the absolute reaction cross sections for the production of SH^+ (m/q=33) and SD^+ (m/q=34) have been extracted to be compared to theoretical predictions.

The potential energies extracted from the set of analytical PESs employed in this work are reported in the correlation energy diagram of the H_2S^+ presented in figure 2. It appears that the production of SH^+ is endoergic by 0.885 eV. We can also see that two electronic states of H_2S^+ (X^2A'' and A^2A') correlating with excited electronic states of S^+ present deep wells and cross the quartet state. One of them also correlates with SH^+ ground state, but since they present a different spin multiplicity, their contribution to reaction is spin-forbidden. To shed light on the mechanism, reactions dynamics have been studied with WP calculations using three models. One considers only the quartet state where the spin-allowed mechanism will take place. The second takes into account both $^4A''$ and $^2A''$, and corresponds to the model proposed by Stowe *et al.*[28]. The third considers additionally the $^2A'$ state to determine its possible role in the reaction mechanism. In case of coupled states, two sets of independent calculations are performed separately for the electronic projections $\Omega = \Lambda + \Sigma = 3/2$ and $1/2$ to obtain their respective cross section. The total cross section of the reaction is then obtained as an average of the two (see section III for details).

The calculated cross sections for the formation of SH^+/SD^+ products are shown in Fig. 4, Fig. 5 and Fig. 6 together with the experimental data measured in this work. Available experimental data on HD and D_2 obtained previously by Stowe *et al.*[28] are also shown for comparison as well as the limits of collision energies below which no discrimination of products are expected (see experimental section).

In the case of H_2 (Fig. 4), a good agreement is observed between theory and experiment. The experimental onset, affected by the broadening of the distribution of collision energy in the molecular beam and the thermal dispertion of the target gas, is in agreement with theoretical predictions around 0.9 eV. In both cross sections, the maximum of the shoulder around 1.7 eV and the subsequent minimum around 2.1 eV can be appreciated. The absolute maximum of the cross section peaks at 0.95 Å^2

TABLE I. Parameters used in the wave packet calculations (all distances are given in Å).

Scattering coordinate:	$R_{\min} = 0.001; R_{\max} = 16.0$
Number of grid points in R:	400
Diatomic coordinate:	$r_{\min} = 0.1; r_{\max} = 16.0$
Grid points in r :	240
No. of angular functions (H_2, D_2) :	160
No. of angular functions (HD) :	260
Initial wave packet position:	$R_0 = 9.0$
Initial kinetic energy/eV :	$E_c = 1.4$
Analysis distance:	r_∞=8.0
Chebyshev iterations:	100000

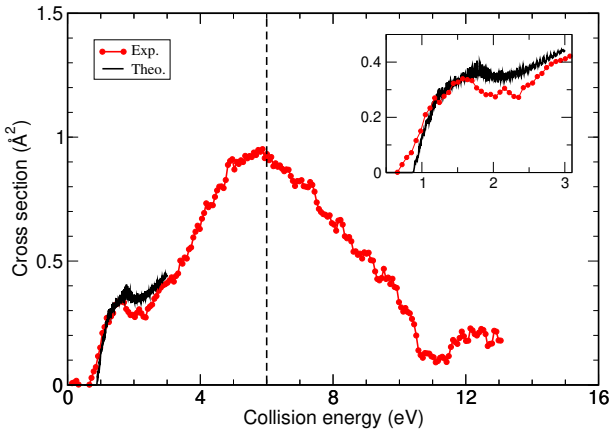

FIG. 4. Integral cross section for the reaction $S^+ + H_2 \rightarrow SH^+$. Red lines corresond to the experimental data from this work and black lines to the WP cross sections of formation of SH^+. The vertical dashed line represent the ECM limit below which no discrimination of products occurs, as explained in the text. An expanded view of the range 0-3 eV is also shown.

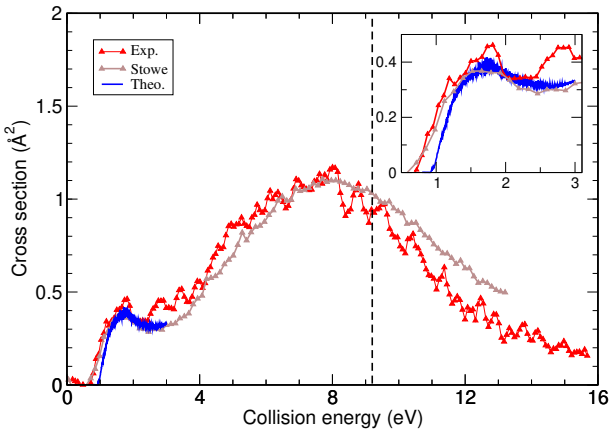

FIG. 5. Integral cross section for the reaction $S^+ + D_2 \rightarrow SD^+$. Brown lines correspond to the experimental cross sections for from Stowe *et al.* [28], red lines to the experimental data from this work, and blue lines to the WP cross sections of formation of SD^+. The vertical dashed line represent the ECM limit below which no discrimination of products occurs, as explained in the text. An expanded view of the range 0-3 eV is also shown.

at a collision energy of 6 eV.

In the case of D_2 (Fig. 5), the cross sections exhibit similar features. As in the case of H_2, two maxima are clearly observed, the lower one between 1 and 2 eV is associated to the spin-forbidden mechanism, and the larger one peaking at 6 eV for H_2 and 8 eV for D_2 to the spin-allowed mechanism. Small diffrences are however observed in the cross section. The maximum of the shoulder and the subsequent minimum can be appreciated more clearly than in the case of H_2. This is because in the case of D_2, the maximum appears at slightly lower collision energy (1.6 eV) while the minimum is observed at larger collision energy (2.6 eV), making the shoulder visually more apparent. The new measurements, although exhibiting a larger dispersion (attributable to a more limited acquisition time), compare well with the previous experiment and with the theoretical predictions. Here again, the experimental onset agrees with theory. We should emphasize the remarkable agreement between calculations and the experimental results of Stowe *et al.* [28]. It is also worth to notice that calculations and both experiments are able to detect these features on the cross sections of SH^+ and SD^+ that do not exceed 0.5 Å^2 in this energy range. Both experiments agree also on the maximum of the cross section which is found to peak at 1.1 Å^2 around 8 eV. Above 10 eV, our measured cross sections in the 10-13 eV Ecm range begin to deviate from Stowe *et al.* [28] and are slightly lower, this could be the sign of the beginning of product discrimination in our experiment at these energies.

The picture is significantly different in the case of HD (Fig. 6). In this case, the cross section is larger than in the previous cases and the first maximum associated to the spin-forbidden mechanism does not appear. Addi-

tionally, a strong propensity toward SD^+ is observed. Although a notable discrepancy on the intensity is observed between the two experimental data sets, the agreement is very good at lower collision energies and the absolute difference in all the energy range remains low (less than 25%). Only above 12 eV, the difference is more visible for both products, SH^+ and SD^+, which vanish in our experimental work. This could be the consequence of some product discrimination in our experiment at these highest collision energies. Below 10 eV, the differences observed with the HD data by Stowe *et al.*[28] are more surprising, in particular in view of the good agreement between the two data sets for the reaction with D_2. Our evaluations of the discrimination of the product ions clearly rule out that the observed difference could be due to any loss of products below 8-10 eV as explained above. A possible explanation could be linked to some contamination of CS_2 (the precursor used to generate S^+) by a leak of O_2 during the acquisition of this particular data set. The presence of O_2 in the source would generate some O_2^+ ions at the same mass as S^+ and therefore contribute to the parent ion signal at mass 32, and consequently affect the ratio products over parents leading to an underestimation of the cross sections. The fact that only the parent signal is strongly affected can be rationalized by the fact that the O_2^++H_2 reaction to produce O_2H^+ is even more endothermic than the title reaction (around 2 eV) and is known to be inefficient[64], so very small production of O_2H^+/O_2D^+ is expected, even if large quantities of O_2 were present in the source. Another interesting feature is that the cross section of SH^+ exhibits more structures than the one of SD^+. It is not clear however if these structures are reflecting a perturbation of competing processes (electronic excitation of S^+ or H_2 fragmentation), or simply structures attributable to statistical noise (the cross section being extremely low, very large number of events should have been counted to statistically converge the result but this was not possible in the limited beam time at synchrotron). This underlines the technical difficulty to measure extremely low absolute reactive cross sections with different possible products in the case of very light neutral targets at high collision energies.

The calculations agree very well with both experiments for the cross section of SH^+, but a better agreement is observed with the cross section of Stowe *et al.*[28] in the case of SD^+. Despite this, both experiments agree on the fact that the maximum of the cross section of SD^+ is found at 6 eV, and an excellent agreement is observed below 1.5 eV and in particular for the onset. Interestingly, the shoulder that appears clearly in the cross sections of the homonuclear cases seems to disappear for HD. We remind that this shoulder was previously attributted to spin-orbit effects[28]. That will be examined below. In order to interpret these results, the Minimum Energy Paths (MEPs) obtained in bond coordinates for a fixed angle of 90^o between HH and SH bonds for the three adiabatic states are shown in figure 7, together with the SOCs in the middle panel. All the couplings are different from

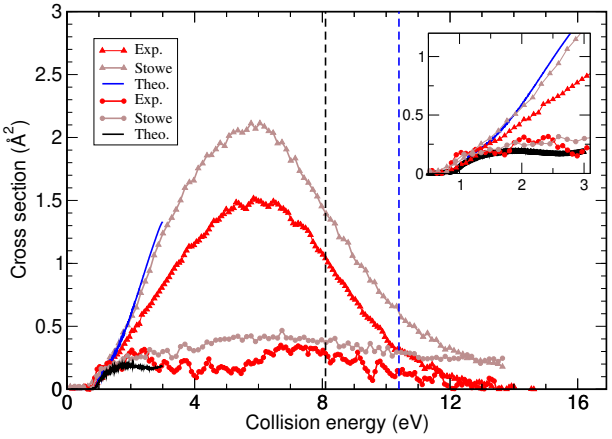

FIG. 6. Integral cross section for the reaction and S^++HD → SH^+/SD^+. Triangles refer to SD^+ while circles refer to SH^+. Brown lines correspond to the experimental cross sections for from Stowe *et al.*[28], red lines to the experimental data from this work, black lines to the WP cross sections of formation of SH^+ and blue lines to the WP cross sections of formation of SD^+. The vertical dashed lines represent the ECM limit below which no discrimination of products occurs, as explained in the text. The black dashed line refers to SH^+ limit and blue dashed line refers to SD^+ limit. An expanded view of the range 0-3 eV is also shown.

zero along the MEPs, except the $^4A''-{}^2A''$ which vanish for $R_{HH} - R_{SH} > 2$ bohr. This occurs because the $^2A''$ state is essentially of Π character when S^+ approaches H_2 and switch to a Σ character when the H_2 bond aparts (see Fig. 3 and associated discussion in section III). Since the SOCs are small compared to the global energies involved in the reaction, it is instructive to look at the coupling divided by the energy differences of the states involved to analyze their impact in the reaction dynamics. Clearly, the quartet-doublet couplings are most effective at the crossings, and the coupling between the two doublets is important in the reactant channels while they are close in energy. Interestingly, not only the region of efficiency of doublet-doublet couplings is wider, but it overlaps with the one where quartet-doublet couplings are also effective, strongly suggesting that both doublet states will have an impact on the ISC. This is further confirmed by analyzing in details the reaction dynamics results.

The effect of the potentials and couplings in the dynamics is seen in the reaction probabilities in each individual electronic state, $^4A''$ and $^2A''$, correlating with the $SH^+(^3\Sigma^-)$ product, as shown for H_2 in Fig. 8. As an illustration, the probabilities obtained are plotted for partial waves J=0 and J=40 considering only one ($^4A''$ in the bottom panels), two ($^4A''$ and $^2A''$ in the middle panels) and three ($^4A''$, $^2A''$ and $^2A'$, top panels) states. When only $^4A''$ state is included, the reaction probability shows a smooth increase with energy, typical of endothermic reaction, which for $J = 40$ is shifted towards higher energy due to the higher rotational barrier.

When the X^2A'' state is included (middle panels), the

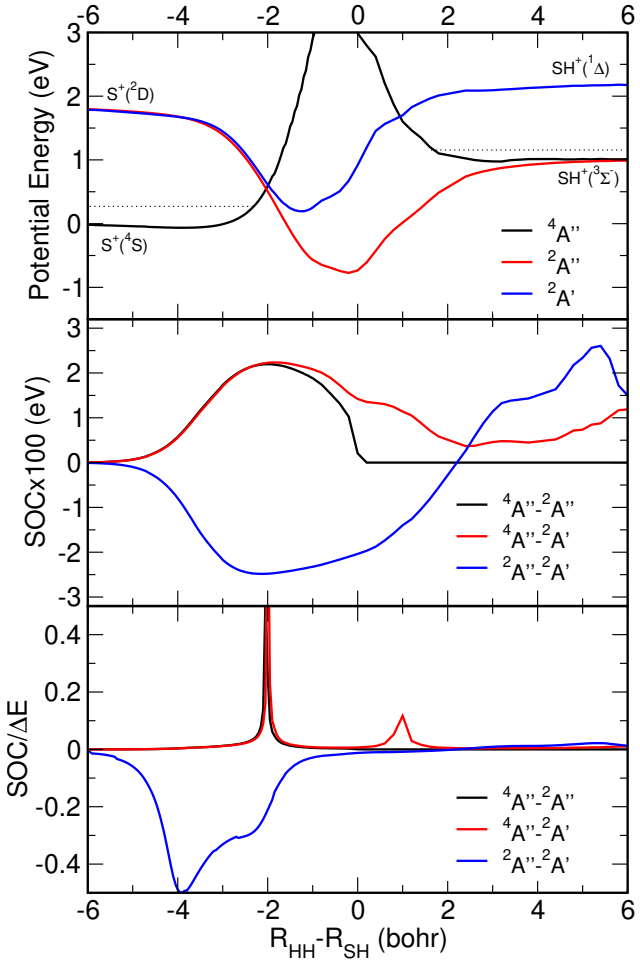

FIG. 7. MEPs (top panel), spin-orbit couplings (middle panel) and spin-orbit couplings divided by electronic energy differences (bottom panel) as a function of the reaction coordinate ($R_{HH} - R_{SH}$) for the H_2+S^+ reaction at 90°. The couplings shown correspond to the electronic projection $\Omega = 3/2$, while those of the $\Omega = 1/2$ are very similar, but divided approximately by a factor of two. The dotted lines in top panel indicates the ZPE of the corresponding dissociation channels.

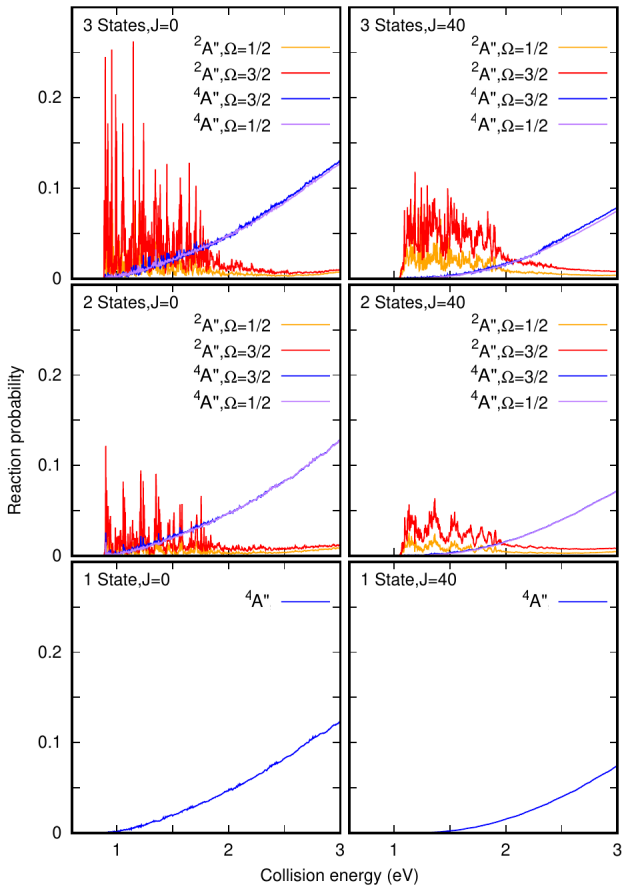

FIG. 8. Probabilities for the S^++H_2 reaction as a function of collision energy on each individual electronic state for total angular momentum $J = 0$ (left panels) and $J = 40$ (right panels) obtained using three models: only $^4A''$ (bottom panels), $^4A''$ and $^2A''$ (middle panels) and $^4A''$, $^2A''$ and $^2A'$ states (top panels).

final probability on the $^4A''$ is very similar to that obtained in the one-state case. The X^2A'' state which also correlates to $SH^+(^3\Sigma^-)$ products but can be accessed only through ISC, shows smaller probabilities that are dominated by resonances in the 1-2 eV energy interval, becoming considerably low for energies higher than 2 eV. The same progression is observed for Ω= 3/2 and 1/2, except that for the latter the probabilites are lower due to weaker couplings intensities. Clearly, the resonant structures can be attributed to quasi-bound states supported by the deep well in the X^2A'' state.

Interestingly, the reaction probability threshold in the X^2A'' state appears at lower energies than that in the $^4A''$ state. This occurs because the $^4A''$ state presents a barrier outside colinearity, as shown in Fig. 7, that reduces the cone of acceptance towards the products, shifting the probability towards higher energy. When increasing total angular momentum J from 0 to 40, a centrifugal barrier induces a shift of the reaction probabilities toward higher energies. The shift in the X^2A'' is only of ≈ 0.2 eV, while a shift of ≈ 0.5 eV is observed for the $^4A''$ state. This can be rationalized by the position of the effective barriers. While the bottleneck of the reaction on the quartet is associated with the barrier to products channel, for the X^2A'' state it is mediated by the quartet-doublet minimum energy crossing point (MECP), where the electronic transition is more likely to occur. Since the MECP is located at considerably larger distance than the reaction barrier, the centrifugal effects lead to a lower rotational barrier and consequently energy shifts. This low rotational barrier makes that the resonant structure persists in the same energy region up to rather high J, giving place to a broad band in the reaction cross section after the partial wave summation. However, as illustrated in Fig. 9, when only the two A'' states are considered, the shoulder remains too low as

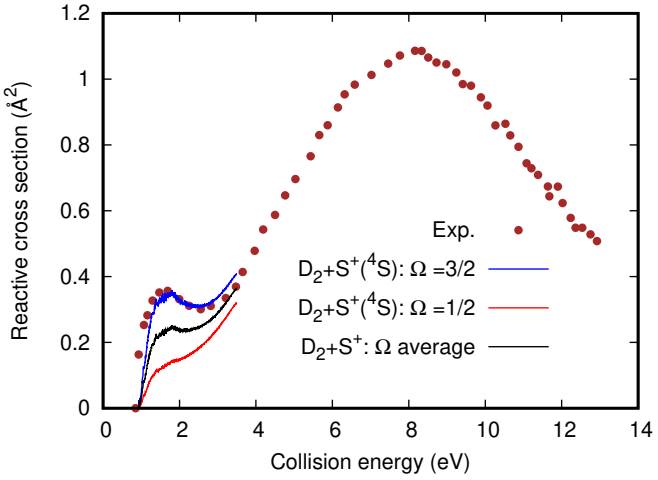

FIG. 9. Integral cross section of the S^++D_2 calculated with the two state model compared to the experiement of Stowe *et al.*[28]. The cross sections associated to $S^+(^4S_{\Omega=3/2})$ and $S^+(^4S_{\Omega=1/2})$ are shown.

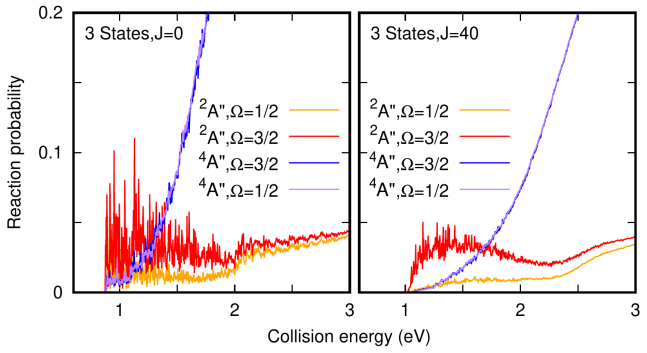

FIG. 10. Probabilities for the S^++HD→ SD^++H reaction as a function of collision energy on each inidividual electronic state for total angular momentum $J = 0$ (left panels) and $J = 40$ (right panels) obtained using the three state models.

compared to the experimental one, while located in the same position.

This clearly indicates that it is absolutely necesary to include the third state, $^2A'$, in order to get good agreement with the experimental cross section. This is not expected at a first glance since this state correlates to excited states of both reactant and products, and cannot contribute directly to $SH^+(^3\Sigma^-)$ formation in the energy range of the shoulder. However, as stated above, this state is not only coupled with the $^4A''$, but it is also coupled with the $^2A''$ state by spin-orbit couplings. Since the two doublets states present deep wells and are coupled, some resonances are shared, allowing effective population transfer between them. This is reflected by the substential increase of resonances intensity in the reaction probabilities that can be appreciated by comparing top and middle pannels of Fig. 8. The portion of the WP that enters the $^2A'$ state can thus be transfered to the $^2A''$ and where the exit channel can be reached. As a consequence, the reaction probabilities on the X^2A'' increases. The rest of the results are similar to those discussed for the 2-state model. In the 3-state model, the reaction cross sections shown in Fig. 4, Fig. 5 and Fig. 6 exhibit a very nice agreement with the experimental results for all the isotopologues. We should remark that a Renner-Teller effect also allows to couple the doublet states, but it was not considered here as previous tests performed on a diabatic model (not presented) did not show any significant differences compared with the two coupled-states calculations.

It has to be noted that the two doublet states involved never cross each other, while it is usually assumed that population transfer is only effective near crossings. This assumption can be traced back to an empirical classification where potentials crossings enters in the "strong coupling limit", while embedded non-crossing potentials are classified as "weak coupling limit"[8,65]. This classification is based on the work of Englman and Jortner[66], originally designed to explain radiationless decay in solvents. Our results tend to indicate that this classification may lead to erroneous assumption in some cases, specially in the gas phase. There are two main reasons for this in our case. First, even if the states do not cross, in all the entrance channel region they are close enough in energy so the couplings can be effective in a wider area than in the case of a crossing, as illustrated in the lower panel of figure 7. The other reason is that both doublet states present wells much deeper than the energy of reactants (-3 eV and -1 eV respectively). So at the energies where the reaction can take place, the population transferred from the quartet accesses an energetical region of the doublet states with high density of rovibrational states. Consequently, there is a high probability to get rovibrational states which are resonant between the two doublet states, favorising population transfer between them. This is probably why methods like TSH and NA-TST usually fail to provide quantitatively accurate prediction on branching ratios when spin-allowed and spin forbidden mechanisms are competing in gas phase reactions[22]. This kind of approaches should thus be used with caution to describe a reaction mediated by ISC in the gas phase, as they may not yield to accurate results at a quantitative point of view.

The other remarkable result is the cross sections obtained with the reaction of S^++HD. Indeed, while the cross sections of H_2 and D_2 are similar, they increase by nearly a factor three in the case of HD, with a huge propensity towards the formation of SD^+ rather than SH^+. As a consequence, the shoulder associated to the ISC, clearly visible in the case of H_2 and D_2, is washed out in the case of HD. From the WP calculation, it is possible to determine the amount of population reaching the different products regions on each PES. Since in all the calculations, the initial WP is located on the quartet PES, the WP flux captured in the asymptotic region of a doublet PES can be directly related to the ISC. When

comparing the case of HD with the other isotopologues, it appears that the portion of the WP which suffers an ISC is very similar, as can be seen in figure 10. In contrast, the probability of reaching the products on the quartet state increases drastically in the case of HD with respect to H_2 and D_2, showing that the spin-allowed mechanism becomes more favorable. If we look at the model considering only the quartet state (no SOCs), the propensity is even more pronounced, with a yield of nearly 100% of SD^+ production up to collision energies close to 3 eV. This implies that most SH^+ produced in the reaction with HD can be associated to the spin-forbidden mechanisms, since the deep wells present on the doublet PESs will favor a statistical distribution of products between SH^+ and SD^+. This is why the cross section associated to SH^+ is so low.

To understand this strong propensity towards SD^+ observed in the spin-allowed mechanism, it is necessary to remind that the reaction is strongly endothermic, and that large collision energies are required for the reaction to take place. When large collision energies are considered, the collision takes place at high velocities, giving no time for reorientation. This will lead to an impulsion mechanism where the lighter atom is preferentially ejected. Similar behavior was observed at high collision energies in the O^++HD reaction where strong propensity of OD^+ was found.[67] It is also in agreement with the qualitative pairwise model proposed by Stowe *et al.*[28] which also predicts that the SD^+ channel should be strongly favored at high collision energies.

V. CONCLUSIONS

The S^++H_2 reactive collision is a prototypical reaction to study and understand ISC since its cross section present clearly differentated contributions of the spin-allowed and spin-forbidden pathways that can be experimentally measured. In order to fully understand the role played by spin orbit couplings on this prototypical case, the reaction has been studied for three isotopologues of H_2 in a work combining theory and experiment.

The absolute cross sections measured in the experiment performed using a source of pure $S^+(^4S)$ are in good agreement with previous measurements obtained for D_2 and HD. This validates the previous experiments which were performed with a contamination of excited $S^+(^2D)$ in the source, whose contribution to the cross section had to be estimated and substracted. In addition, the absolute cross section for H_2, unavailable in literature, is now presented.

Theorically, a new rigourous approach to account properly for the spin orbit couplings in the reaction dynamics is presented. The resulting couplings were then employed in the time-dependent quantum-mechanical calculations together with the available existing PESs of Zanchet *et al.*[37]. By contrasting the theoretical cross sections, calculated for all isolotopogues assuming 3 different models (uncoupled, 2-states and 3-states coupled), with the experimetal one, we show that accounting for spin-orbit interaction is crucial to reproduce the experimental cross section, thus confirming the spin-forbidden contribution to reaction. We additionally demonstrate that three electronic states are involved in the mechanism of the title reaction, and that ISCs occur between 3 states instead of two as previously thought. More surprisingly, we show that ISC can occur between states of same spin multiplicity when doublets are involved. Finally, we also show that in the gas phase, ISC can be very efficient in the case of embedded potentials, even in absence of MECP.

This last point, which was not considered in the approximations employed to develop methods such as TSH or NA-TST usually employed nowadays to account for spin-orbit effects, explain in part why such methods are unable to reproduce quantitatively ISC processes. It is still not clear how these methods could be improved in order to consider the case of non-crossing embedded potentials, but such improvements are necessary in order to understand properly the role of ISCs in the chemistry of bigger size systems or in the ultracold regime, for which accurate theoretical predictions are hindered due to the computational cost of exact quantum calculations. The use of approximated semi-classical or statistical methods thus remains the most viable option to estimate rate constants for such systems and there is a necessity to improve them. We believe that the new calculations on this prototypical system provided in this work, which are validated by the excellent agreement with experiments, may serve as a benchmark to improve current models and check their validity.

AUTHOR CONTRIBUTIONS

A. Z., O. R. and E. K. performed theoretical calculations. N. S., C. R., R. T. and C. A. collected experimental data. A. Z., C. A. and O. R. conceptualized the project. A. Z. coordinated the project and wrote the manuscript. All authors discussed, commented and revised the manuscript.

ACKNOWLEDGMENTS

We thank P. B. Armentrout for kindly providing us his data on the title reaction. We acknowledge SOLEIL for provision of synchrotron radiation facilities and we would like to thank L. Nahon for assitance in using beamline DESIRS under proposal 20211187. The research leading to these results has received funding from MICINN (Spain) under grants PID2019-107115GB-C21 and PID2021-122549NB-C21. C. A. acknowledge the synchrotron SOLEIL for the support to the associated CERISES setup of ICP since 2008 and subsistence expenses during beamtime periods. AZ thanks the CSIC

institution for the intramural project 202050I028. EK is grateful to the Scientific and Technological Research Council of Turkey for TR-Grid facilities and the grant 1059B191801242 under TUBITAK's 2019-Program. We acknowledge the computing grants from the "Red Española de Super-computación" under grants QH-2021-2-0019 (Calendula), AECT-2021-1-0011 (Cibeles) and AECT-2020-1-0003 (Marenostrum). We also acknowledge the computing time at Grid Computing Centre (TRUBA resources) in Turkey, as well as Drago (CSIC) and Finisterre III (CESGA) in Spain. The COST Action CA21101 (COSY) is also acknowledged.

VI. REFERENCES

[1]H. Li, A. Kamasah, S. Matiska, and A. G. Suits, Nat. Chem. **11**, 123 (2019).
[2]L. Bañares, Nat. Chem. **11**, 103 (2019).
[3]A. R. Mcintosh and J. R. Bolton, Nature **263**, 443 (1976).
[4]J. D. Knoll and C. Turro, Coord. Chem. Rev. **282-283**, 110 (2015).
[5]K. Goushi, K. Yoshida, K. Sato, and C. Adachi, Nat. Photon. **6**, 253 (2012).
[6]H. Wang, S. Jiang, W. Liu, X. Zhang, Q. Zhang, Y. Luo, and Y. Xie, Angew. Chem. Int. Ed. **59**, 11093 (2020).
[7]M. A. El-Sayed, J. Chem. Phys. **38**, 2834 (1963).
[8]T. J. Penfold, E. Gindensperger, C. Daniel, and C. M. Marian, Chem. Rev. **118**, 6975 (2018).
[9]A. H. Zewail, Science. **242**, 1645 (1988).
[10]A. Morita and S. Kato, J. Chem. Phys. **97**, 3298 (1993).
[11]C. Daniel, M.-C. Heitz, J. Manz, and C. Ribbing, J. Chem. Phys. **102**, 905 (1995).
[12]M. Pederzolli and J. Pittner, J. Chem. Phys. **146**, 114101 (2017).
[13]S. Mai, P. Marquetand, and L. Gonzalez, Int. J. Quantum Chem. **115**, 1215 (2015).
[14]G. Cui and W. Thiel, J. Chem. Phys. **141**, 124101 (2014).
[15]P. Mondal and W. Domcke, J. Phys. Chem. A **118**, 3726 (2014).
[16]C. Xie, X. Hu, L. Zhou, and H. Guo, J. Chem. Phys. **139**, 014305 (2013).
[17]J. N. Harvey, Wiley Interdiscip. Rev. Comput. Mol. Sci. **4**, 1 (2014).
[18]A. O. Lykhin, D. S. Kaliakin, G. E. dePolo, A. A. Kuzubov, and S. A. Vargaov, Int. J. of Quantum Chemistry **116**, 750 (2016).
[19]B. Maiti and G. C. Schatz, J. Chem. Phys. **119**, 12360 (2003).
[20]B. Maiti, G. C. Schatz, and G. Lendvay, J. Phys.Chem. A **108**, 8772 (2004).
[21]T.-S-Chu, X. Zhang, and K.-L. Han, J. Chem. Phys. **122**, 214301 (2005).
[22]P. Casavecchia, F. Leonori, and N. Balucani, Int. Rev. in Phys. Chem. **34**, 161 (2015).
[23]F. Talotta, S. Morisset, N. Rougeau, D. Lauvergnat, and F. Agostini, J. Phys. Chem. A **125**, 6075 (2021).
[24]W. Hu, G. Lendvay, B. Maiti, and G. C. Schatz, J. Phys. Chem. A **112**, 2093 (2008).
[25]B. Fu, Y.-C. Han, J. M. Bowman, L. Angelucci, N. Balucani, F. Leonori, and P. Casavecchia, PNAS **109**, 9733 (2012).
[26]L. Xiaohu, A. W. Jasper, J. Zador, and S. J. Klippenstein, Proc. of the Comb. Inst. **36**, 219 (2017).
[27]G. R. Satchler, Nuc. Phys. **21**, 116 (1960).
[28]G. F. Stowe, R. H. Shultz, C. A. Wight, and P. B. Armentrout, Int. J. Mass Spectr. and Ion Proc. **100**, 177 (1990).
[29]R. N. Dixon, G. Duxbury, M. Horani, and J. Rostas, Mol. Phys. **22**, 977 (1971).
[30]G. Duxbury, M. Horani, and J. Rostas, Proc.R. Soc. Lond. A **331**, 109 (1972).
[31]G. R. Möhlmann and F. J. D. Herr, Chem. Phys. Lett. **36**, 353 (1975).
[32]P. Baltzer, L. Karlsson, M. Lundqvist, B. Wannberg, D. M. P. Holland, and M. A. MacDonald, Mol. Phys. **195**, 403 (1995).
[33]Z. Luan, Y. Fu, Y. Tan, Y. Wang, B. Shan, J. Li, X. Zhou, W. Chen, L. Liu, B. Fu, D. H. Zhang, X. Yang, and X. Wang, J. Phys. Chem. Lett. **13**, 8157 (2022).
[34]A. Zanchet, M. Agúndez, V. J. Herrero, A. Aguado, and O. Roncero, Astronom. J. **146**, 125 (2013).
[35]A. Zanchet, O. Roncero, and N. Bulut, Phys. Chem. Chem. Phys. **18**, 11391 (2016).
[36]Y. Z. Song, Y. Zhang, B. Gao, Q. T. Meng, C. K. Wang, and M. Y. Ballester, Mol. Phys. **116**, 129 (2018).
[37]A. Zanchet, F. Lique, O. Roncero, J. R. Goicoechea, and N. Bulut, A&A **626**, A103 (2019).
[38]Z. Zhu, A. Zhang, D. He, and W. Li, Phys. Chem. Chem. Phys. **23**, 4757 (2021).
[39]W. Y. Zhang, Q. T. Meng, S. B. Gao, and Y. Z. Song, Chem. Phys. Lett. **764**, 138257 (2021).
[40]J. Bai, F. Yuan, and Y. Zhang, Eur. Phys. J. D **76**, 10 (2022).
[41]Y. Sun, W. Li, and M. Yuan, Chem. Phys. Lett. **833**, 140931 (2023).
[42]B. K. Cunha de Miranda, C. Romanzin, S. Chefdeville, V. Vuitton, J. Zabka, M. Polasek, and C. Alcaraz, J. Phys. Chem. A **119**, 6082 (2015).
[43]C. Alcaraz, C. Nicolas, R. Thissen, J. Zabka, and O. Dutuit, J. Phys. Chem. A **108**, 9998 (2004).
[44]L. Nahon, N. de Oliveira, G. Garcia, J. F. Gil, B. Pilette, O. Marcouille, B. Lagarde, and F. Polack, J. Synchrotron Rad. **19**, 508 (2012).
[45]K. M. Ervin and P. A. Armentrout, J. Chem. Phys. **83**, 166 (1985).
[46]H.-J. Werner, P. J. Knowles, R. Lindh, M. Schütz, P. Celani, T. Korona, F. R. Manby, G. Rauhut, R. D. Amos, A. Bernhardsson, A. Berning, D. L. Cooper, M. J. O. Deegan, A. J. Dobbyn, F. Eckert, C. Hampel, G. Hetzer, A. W. Lloyd, S. J. McNicholas, W. Meyer, M. E. Mura, A. Nicklass, P. Palmieri, R. Pitzer, U. Schumann, H. Stoll, A. J. Stone, R. Tarroni, T. Thorsteinsson, and M. Wang, "Molpro, version 2012, a package of ab initio programs," See http://www.molpro.net.
[47]H.-J. Werner and P. J. Knowles, J. Chem. Phys. **82**, 5053 (1985).
[48]H.-J. Werner and P. J. Knowles, J. Chem. Phys. **89**, 5803 (1988).
[49]A. Berning, M. Schweizer, H.-J. Werner, P. J. Knowles, and P. Palmieri, Mol. Phys. **98**, 1823 (2000).
[50]T.-S. Ho and H. Rabitz, J. Chem. Phys. **104**, 2584 (1996).
[51]P. Gamallo, A. Zanchet, F. J. Aoiz, and C. Petrongolo, Phys. Chem. Chem. Phys. **22**, 17091 (2020).
[52]A. Zanchet, B. Bussery-Honvault, and P. Honvault, J. Phys. Chem. A **110**, 12017 (2006).
[53]A. Zanchet, B. Bussery-Honvault, M. Jorfi, and P. Honvault, Phys. Chem. Chem. Phys. **11**, 6182 (2009).
[54]A. Aguado, M. Paniagua, M. Lara, and O. Roncero, J. Chem. Phys. **106**, 1013 (1997).
[55]M. Paniagua, A. Aguado, M. Lara, and O. Roncero, J. Chem. Phys. **109**, 2971 (1998).
[56]A. Aguado, M. Paniagua, C. Sanz-Sanz, and O. Roncero, J. Chem. Phys. **119**, 10088 (2003).
[57]T. González-Lezana, A. Aguado, M. Paniagua, and O. Roncero, J. Chem. Phys. **123**, 194309 (2005).
[58]S. Gómez-Carrasco and O. Roncero, J. Chem. Phys. **125**, 054102 (2006).
[59]A. Zanchet, O. Roncero, T. González-Lezana, A. Rodríguez-López, A. Aguado, C. Sanz-Sanz, and S. Gómez-Carrasco, J. Phys. Chem. A **113**, 14488 (2009).
[60]A. Zanchet, T. González-Lezana, A. Aguado, S. Gómez-Carrasco, and O. Roncero, J. Phys. Chem. A **114**, 9733 (2010).
[61]A. Aguado, M. Paniagua, M. Lara, and O. Roncero, J. Chem. Phys. **107**, 10085 (1997).
[62]M. Lara, A. Aguado, O. Roncero, and M. Paniagua, J. Chem. Phys. **109**, 9391 (1998).

[63] A. Zanchet, M. Agúndez, V. J. Herrero, A. Aguado, and O. Roncero, The Astronomical Journal **146**, 125 (2013).
[64] B. H. Mahan, M. H. Chiang, E. A. Gislasson, C. W. Tsao, and A. S. Werner, J. Phys. Chem. **75**, 1426 (1971).
[65] F. Thorning, P. Henke, and P. R. Ogilby, J. Am. Chem. Soc. **144**, 10902 (2022).
[66] R. Englman and J. Jortner, Mol. Phys. **18**, 145 (1970).
[67] N. Bulut, O. Roncero, and F. Lique, J. Phys. Chem. A **124**, 6552 (2020).